Cooperativity of a Protein Folding Reaction Probed at Multiple Chain Positions by Real-Time 2D NMR Spectroscopy†

Clemens Steegborn,‡ Henriette Schneider-Hassloff, Markus Zeeb, and Jochen Balbach*

Laboratorium für Biochemie, Universität Bayreuth, D-95440 Bayreuth, Germany

Received February 4, 2000; Revised Manuscript Received April 20, 2000

ABSTRACT: The refolding reaction of S54G/P55N ribonuclease T1 is a two-step process, where fast formation of a partly folded intermediate is followed by the slow reaction to the native state, limited by a trans → cis isomerization of Pro39. The hydrodynamic radius of this kinetic folding intermediate was determined by real-time diffusion NMR spectroscopy. Its folding to the native state was monitored by a series of 128 very fast 2D ^{15}N-HMQC spectra, to observe the kinetics of 66 individual backbone amide probes. We find that the intermediate is as compact as the native protein with many native chemical shifts. All 66 analyzed amide probes follow the rate-limiting prolyl isomerization, which indicates that this cooperative refolding reaction is fully synchronized. The stability of the folding intermediate was determined from the protection factors of 45 amide protons derived from a competition between refolding and H/D exchange. The intermediate has already gained 40% of the Gibbs free energy of refolding with many protected amides in not-yet-native regions.

The principles of how a polypeptide chain finds its biologically active conformation under native conditions are still not understood. A growing group of small proteins fold very fast, within tens of milliseconds or faster, following a simple two-state reaction (*1*). For most proteins, however, intermediates accumulate transiently during refolding. These intermediates are believed to contain crucial information about the folding mechanism, but a detailed characterization of their structures proves to be extremely difficult. At present, there is a controversial discussion, whether these intermediates are obligatory 'on-pathway' species, whether they are kinetically trapped 'off-pathway' species, which might even prevent efficient fast folding, or whether they represent only local minima on a rough predetermined energy landscape (the 'new view' of protein folding).

An ingenious approach to study protein folding intermediates focused on amide protons that are protected from exchange with the solvent by structured elements, already present in the folding intermediate (*2*−*5*). These pulse labeling experiments performed in quenched-flow apparatuses with subsequent NMR analysis allowed a characterization of very early states of folding, in a typical time range of 5 ms to 2 s. The time course of structure formation could be derived by varying the refolding time before the labeling pulse. For a quantitative analysis of the local stability of intermediates, protection factors have to be determined either by altering the pH of the labeling pulse at constant refolding times (*6*) or by a competition between refolding and H/D exchange (*7, 8*).

Recently, time-resolved 1D and 2D NMR techniques were developed to study protein folding reactions at high structural resolution [see references in review (*9*)]. Dead times for these real-time NMR experiments range from 100 ms to 4 s, and the time resolution in 1D measurements is about 1 s per spectrum. Kinetic information can be derived by integration of well-resolved resonances of single nuclei in successively recorded 1D spectra or by line shape analysis in 2D spectra (*10, 11*).

The determination of cooperative events in protein folding is limited by the fact that with most methods only few molecular reporters are available or a single averaged signal is obtained for many sites. These methods include fluorescence spectroscopy of aromatic side chains, far- and near-UV CD spectroscopy, and 1D NMR spectroscopy with unlabeled protein. To increase the number of directly detectable site-specific probes, selected residues can be labeled (*12*), which might become very time-consuming for a global analysis. We used instead in the present study uniformly ^{15}N-labeled ribonuclease T1 variant S54G/P55N and fast 2D NMR spectroscopy (*13*) and could analyze for this slow folding reaction the time dependency of 91 resolved resonances from both the folding intermediate and the native state.

S54G/P55N ribonuclease T1 (S54G/P55N-RNase[1] T1) follows a simplified refolding mechanism compared to the

† This research was supported by grants from the Deutsche Forschungsgemeinschaft (Ba 1821/1-1, Ba 1821/2-1) and from the Fonds der Chemischen Industrie (Li 153/2 Bio).

* Correspondence should be addressed to this author at Biochemie III, Universität Bayreuth, D-95440 Bayreuth, Germany. Tel.: ++49 921 553663. FAX: ++49 921 553661. E-mail: jochen.balbach@uni-bayreuth.de.

‡ Present address: MPI für Biochemie, Am Klopferspitz 18a, 82152 Planegg-Martinsried, Germany.

[1] Abbreviations: RNase T1, ribonuclease T1 from *Aspergillus oryzae*; S54G/P55N-RNase T1, variant of RNase T1 with substitutions Ser54→Gly and Pro55→Asn; GdnHCl, guanidine hydrochloride; GdnDCl, guanidine deuterochloride; U, I, and N represent the unfolded, the intermediate, and the native state, respectively; pH*, pH-meter reading in D_2O buffer without isotope correction; HMQC, heteronuclear multi quantum coherence; HSQC, heteronuclear single quantum coherence; R_h, hydrodynamic radius; R_g, radius of gyration.

10.1021/bi000270u CCC: $19.00
Published on Web 06/16/2000

wild-type protein, because it has only one remaining cis peptide bond (*14*, *15*):

$$U^{39c} \xrightarrow{\text{fast}} N^{39c}$$

$$U^{39t} \xrightarrow{\text{fast}} I^{39t} \xrightarrow{\text{slow}} N^{39c}$$

About 15% of the unfolded molecules with intact disulfide bonds (U^{39c}) contain this peptide bond, Tyr38−Pro39, in the native cis conformation and therefore refold with a time constant of about 200 ms. Under strong refolding conditions, most of the remaining 85% unfolded molecules (U^{39t}) rapidly form a folding intermediate (I^{39t}) with a non-native trans prolyl peptide bond at position 39. Its very slow trans → cis isomerization is the rate-limiting step in the conversion of the intermediate to the native state N^{39c} (*14*, *16*). This intermediate is thus long-lived and very well suited for a study with high-resolution methods such as NMR spectroscopy (*11*).

In this paper, we characterize the protein folding intermediate of S54G/P55N-RNase T1 regarding its hydrodynamic radius, its backbone chemical shifts, its refolding cooperativity based on refolding rates derived from 66 individual amide protons of the native state, and its thermodynamic stability calculated from the protection factors of 45 amide protons. The hydrodynamic radius of the intermediate was determined by time-resolved diffusion experiments during the refolding reaction from 6 M GdnHCl. To obtain folding kinetics from all sites of the protein, we used a very fast ^{15}N-HMQC technique (*13*) to record a series of 128 2D experiments during the refolding experiment. From these time-resolved data, we could also identify native and not-yet-native regions in the intermediate based on the chemical shift information. Finally, a competition between refolding and hydrogen−deuterium exchange with the solvent was used to derive the protection factors of amide protons in all secondary structure elements in the intermediate, revealing its local and global stability.

MATERIALS AND METHODS

Materials. GdnHCl (ultrapure) was purchased from ICN Biomedicals (Eschwege, Germany); all other chemicals from Merck (Darmstadt, Germany). GdnDCl was prepared by 4 times dissolving GdnHCl in an excess of ^2H_2O and subsequent lyophilization.

Purification of S54G/P55N-RNase and Labeling with ^{15}N. S54G/P55N-RNase T1 was expressed in *Escherichia coli* DH5α cells transformed with plasmid pAT1S54G/P55N carrying the gene for the RNase T1 variant (*17*). The overexpressed protein was purified as described previously (*18*). For uniformly labeling S54G/P55N-RNase T1 with ^{15}N, *Escherichia coli* DH5α/pAT1S54G/P55N was grown in M9 minimal medium supplemented with 4 mg/mL glucose, 10 μg/mL thiamin hydrochloride, and 1 mg/mL $^{15}NH_4Cl$. The following purification was done as described previously (*18*).

Assignment of ^{1}H and ^{15}N Resonances of S54G/P55N-RNase. NMR spectra were recorded with samples containing 0.7 mM S54G/P55N-RNase T1 in 10 mM oxalate, pH 5.0, 0.6 M GdnHCl at 25 °C. These conditions were chosen because they match the final conditions after the time-resolved NMR refolding experiments. Assignment of resonances was achieved using homonuclear 2D COSY, TOCSY, and NOESY spectra, as well as 3D NOESY−^{15}N-HSQC and 3D TOCSY−^{15}N-HSQC experiments recorded with ^{15}N-labeled S54G/P55N-RNase T1. All these data including the real-time diffusion and real-time 2D ^{15}N-HMQC experiments (see below) were recorded at a DRX 600 spectrometer (Bruker) equipped with a pulsed field gradient unit. Quadrature detection in the indirect dimension was achieved either by States-TPPI (*19*) or by the echo−antiecho method when gradients were used for coherence selection (*20*). Typical spectral widths were 16 ppm (^{1}H) and 34 ppm (^{15}N). Data processing and resonance assignments were performed using the programs NDEE (Symbiose) and Felix (MSI).

Real-Time NMR Experiments during the Refolding of S54G/P55N-RNase T1. All time-resolved refolding experiments were initiated inside the NMR spectrometer by a rapid 10-fold dilution of 7 mM unfolded protein in 6 M GdnHCl or GdnDCl (for the competition experiment) in the respective protonated or deuterated refolding buffer containing 10 mM sodium oxalate, pH 5.0, as described earlier (*11*). GraFit 3.0 (Erithacus Software) was used for all fittings of the theoretical functions to the respective NMR intensities.

For the time-resolved diffusion experiment, a set of 189 PFG-SLED gradient echo experiments (*21*, *22*) was performed during the refolding experiment at 1 °C. For each set, 10 equally spaced gradient strengths between 10% and 100% of the maximum value were used for the 10 ms de- and refocusing gradients along the *x*-axis followed by a 1 ms recovery delay. All other delays and pulses, including a diffusion delay of 41 ms and 1 ms spoil gradients along the *y*-axis during the diffusion delay and along the *z*-axis before data acquisition, were kept constant. Therefore, the integral of the NMR intensity, $I(g,t)$, between 0.42 and 1.60 ppm with exact equal contributions of the native and intermediate states [determined from the 1D real-time NMR experiment (*11*)] is represented by eq 1:

$$I(g,t) = p_I(t)A_I \exp[-d_I g(t)^2] + p_N(t)A_N \exp[-d_N g(t)^2] \quad (1)$$

with

$$p_I(t) = \exp(-tk) \text{ and } p_N(t) = 1 - \exp(-tk)$$

Differences in the amplitudes A_I and A_N of the intermediate and the native state, respectively, are mainly due to different T_1 relaxation during the diffusion delay of these states. d_I and d_N are proportional to the diffusion constants of states I and N, respectively. As all delays were kept constant, the constant of proportion is the same for I and N. Therefore, the ratio d_I/d_N reflects the ratio of the diffusion constants, and referencing to the internal standard dioxane (*22*) is not necessary. It should be noted that the time resolution is 10 times better than 189 complete diffusion datasets (with 10 gradient strengths from 10% to 100%) during the entire refolding experiment, because the gradient strength at every time point t is relevant in eq 1. The populations p_N of the native state and p_I of the intermediate state are given by $p_N = 1 - 0.18 \exp(-tk)$ and $p_I = 0.82 \exp(-tk)$. k was determined independently to be 27835 s, and the offset due to the second fast folding track was 18% by analyzing the well-resolved native H^δ proton of I90 at −1.20 ppm in the same dataset.

It was shown earlier that a second mainly unstructured intermediate is populated transiently by about 7% of the refolding molecules with a much faster relaxation time (*11*, *14*). The performed diffusion experiment is a time average over the ensemble of states present. This ensemble has on average a reduced hydrodynamic radius, which is close to the native state and the last 5% of reduction accompanies the rate-limiting step. The second minor intermediate decays about 10 times faster than the major intermediate studied in this paper. Fitting eq 1 to the dataset after 4000 s, when the minor intermediate is not populated anymore, gives the same relative diffusion constant, indicating a minor contribution of the second intermediate.

For the 2D real-time NMR experiment, a series of 128 fast 2D ^{15}N-HMQC spectra (*13*) were recorded with 32 complex points in the ^{15}N(t_1) dimension and a spectral width of 34 ppm. To increase the repetition rate between scans, the delay t_{max} for FID acquisition and relaxation was reduced to 500 ms. During this delay, only 50% of the protein magnetization has relaxed to $+Z$ with an averaged apparent T_1 time of 725 ms, determined from an inversion−recovery experiment. Therefore, the pulse angle β for the first excitation pulse was set to 120°. Under our experimental conditions, the signal/noise ratio in 2D ^{1}H−^{15}N correlation spectra recorded for a definite length of time was found to be best with the presented pulse sequence as compared to standard HMQC or sensitivity-enhanced HSQC experiments (*23*, *24*).

The signal intensities rather than volume integrals of the respective cross-peaks were determined from this series of 2D spectra. For those 22 resonances which have native chemical shifts in the intermediate, it is very unlikely that they result from an overlap by a resonance with exactly the same chemical shift and the same intensity, which would mimic a native signal in the intermediate. First, these identified residues showed native NOE effects in the 2D real-time NOESY experiment (*11*) if there was an unambiguous amide proton to be analyzed. Second, for some cross-peaks, the intensity increases or decreases with time with amplitude offsets between 30% and 90% but without changes in the time constants. These resonances must be disturbed by overlapping signals. For four residues in the C-terminal part of the α-helix (D15−T18), which showed mainly native NOE effects in the 2D real-time NOESY spectrum, two overlapping cross-peaks of I and N could be identified in the HMQC, which could not be resolved in the homonuclear 2D real-time NOESY spectrum due to degenerated proton chemical shifts. Integration of the whole overlapping cross-peak gave again a constant intensity with time. Therefore, we count these four residues to the class of native-like in the intermediate as well. Severe changes in the intensities due to differences in the exchange rates with saturated water between the native and the intermediate state can be excluded, because a water flip-back HMQC method was used.

Determination of Protection Factors in Native S54G/P55N-RNase T1 and the Intermediate. H/D exchange of native ^{15}N-S54G/P55N-RNase T1 was followed for 13.5 h by a series of 128 2D ^{1}H−^{15}N-HMQC experiments after dissolving 5 mg of protonated protein in 450 μL of D_2O/H_2O (9/1), 0.6 M GdnDCl, 10 mM sodium oxalate, pH* 5.0 (to match exactly the buffer conditions of the competition experiment), equilibrated for 10 min at 25 °C. A single-exponential function was fitted to the respective decaying intensities of the amide cross-peaks.

For the competition between H/D exchange and refolding at 10 °C, 5 mg of protonated ^{15}N-S54G/P55N-RNase T1 was unfolded in 50 μL of 6.0 M GdnHCl, 10 mM sodium oxalate, pH* 5.0. Refolding was initiated by adding 450 μL of D_2O refolding buffer, 10 mM sodium oxalate, pH* 5.0. After 9 h, a 2D ^{1}H−^{15}N-HMQC spectrum was recorded. For the reference HMQC spectrum, the same amount of native protein was dissolved 9 h before data acquisition under the final buffer conditions of the competition experiment. A similar experiment was recorded at pH 4.0 (data not shown).

Intrinsic exchange rates, k_{int}, were calculated with the program HXPep (Z. Zhang) based on the model peptides of Bai et al. (*25*). For the calculations, a trans peptide bond of Y38−P39 was assumed for the intermediate and a cis configuration for the native state.

The change in standard free energy of the opening reaction derived from the protection factor, which is the intrinsic exchange rate k_{int} divided by the observed exchange rate k_{ex}, was calculated by eq 2, valid for an EX2 mechanism of hydrogen exchange with the solvent (*25*):

$$\Delta G^0_{op} = RT \ln(k_{int}/k_{ex}) \quad (2)$$

RESULTS

^{15}N Enrichment and Resonance Assignment of S54G/P55N-RNase T1. For a high-resolution study of transient folding intermediates, two-dimensional NMR experiments are required to resolve spin labels of almost every residue. Therefore, heteronuclear ^{15}N-edited 2D NMR experiments were performed to obtain structural information about the major folding intermediate of S54G/P55N-RNase T1. For this purpose, the protein was uniformly enriched with ^{15}N by expression of S54G/P55N-RNase T1 in *E. coli* fermented in minimal medium supplemented with $^{15}NH_4Cl$. Complete isotope labeling was proven by MALDI-MS (data not shown). ^{1}H and ^{15}N resonances were assigned under the final experimental conditions of our refolding experiments. This was achieved using a three-dimensional ^{15}N−^{1}H-NOESY−HSQC spectrum and a ^{15}N−^{1}H-TOCSY−HSQC spectrum of S54G/P55N-RNase T1 in 10 mM oxalate, pH 5.0, 0.6 M GdnHCl at 25 °C. Ninety of the 104 amide nitrogen resonances and 90 of the 101 amide proton resonances could be unambiguously assigned, using the assignment for wild-type RNase T1 of Pfeiffer et al. (*26*) as a starting point.

Time-Resolved Diffusion Experiments. The translational diffusion constant of a molecule in solution is inversely proportional to its hydrodynamic radius (R_h). Protein diffusion can be measured by NMR spectroscopy with a longitudinal pulsed field gradient echo experiment (*21*, *22*, *27*). Typically, a series of 10−20 1D spectra with different gradient strengths are recorded. Diffusion along the applied field gradient results in a loss of signal intensity. From the signal loss within different gradients, the diffusion constant can be calculated (for details, see Materials and Methods). We combined this technique with a 1D real-time refolding experiment of S54G/P55N-RNase T1 at 1 °C by using the procedure described earlier (*11*) to initiate the refolding reaction in the NMR tube. The folding intermediate is formed

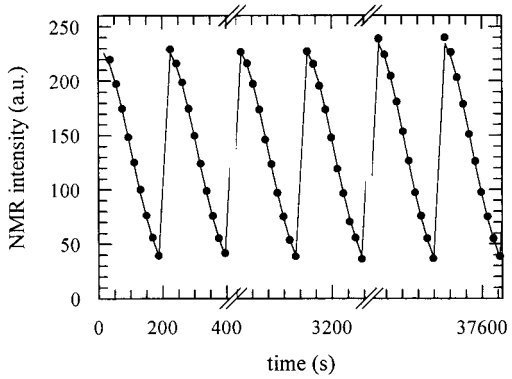

FIGURE 1: Start, middle, and final sections of the time-resolved NMR diffusion experiment recorded during refolding of S54G/P55N-RNase T1, initiated by 10-fold dilution from 6 M GdnDCl in D_2O, pH 5.0, 1 °C. Each filled circle represents the signal integral between 0.42 and 1.60 ppm in the respective 1D spectrum, recorded for 20 s. After 10 incrementations of the gradient strength, it was set back to the first value and repeated 189 times. Six of these 189 datasets are depicted. The solid line was derived by fitting eq 1 to the full dataset with a fix $k = 2.16 \times 10^{-3}$ min^{-1}: $A_I = 227.8 \pm 0.3$; $A_N = 245.7 \pm 0.2$; $d_I = 1.78 \pm 0.01$; $d_N = 1.86 \pm 0.01$.

within the dead time of the experiment and reacts to the native state with a time constant of about 350 min. Therefore, 189 diffusion experiments, each comprising 10 different gradient strengths, could be recorded during the whole refolding reactions. At every time point, both the gradient strength and the populations of the intermediate and the native state are known. Therefore, the diffusion constant of the intermediate relative to the native state can be calculated. The theoretical function (see eq 1 under Materials and Methods) was fitted to the full dataset of integrated NMR intensities between 0.42 and 1.60 ppm. Figure 1 shows the first two diffusion experiments, two experiments after 400 s and the final two datasets.

The diffusion constant of the intermediate is 5% smaller than the diffusion constant of the native state. This indicates that the hydrodynamic radius of the intermediate is only about 5% increased and therefore already very close to the radius of the native protein. Almost the entire compaction of the extended unfolded protein chain thus occurred concomitant to the population of I^{39t} before the rate-limiting folding step.

A second observation confirms the close similarity between the intermediate and the native state. The amplitude of the integral component of the intermediate (A_I in eq 1) is only 7% reduced for the intermediate in comparison to the value for the native protein. The amplitude is mainly determined by the loss of magnetization because of spin relaxation during the 41 ms diffusion delay in the NMR experiment. Therefore, the correlation times of both states must be close as well. This contrasts with the observed amplitudes of intermediates of the molten globule type. For the kinetic molten globule of α-lactalbumin, for example, this amplitude is decreased by 45% albeit the R_h of the intermediate is only 7% increased relative to the native apoprotein (J. Balbach, unpublished data).

2D Real-Time NMR Experiments. To examine the cooperativity of a protein folding reaction, kinetic information from many individual sites of the macromolecule is required. Such a high spatial resolution can, in principle, be obtained by multidimensional NMR spectroscopy. 2D NMR experiments are very time-consuming. Therefore, we used a fast data acquisition method and selected conditions under which the final folding step from the intermediate to the native state is very slow.

Refolding of S54G/P55N-RNase T1 from 6 M GdnHCl after a 10-fold dilution shows a time constant of 7300 s at 10 °C, pH 5.0, and is therefore slow enough to be followed directly by time-resolved 1D NMR spectroscopy with a limited resolution of the resonances (*11*). In the present study, the temperature for the refolding experiment was decreased to 1 °C (time constant ca. 350 min), which allows the reaction to be followed by 2D real-time NMR spectroscopy. Therefore, we could substantially increase the chemical shift resolution of the 1D approach with a series of 128 fast two-dimensional ^{15}N-HMQC experiments (*13*). This technique allows us to decrease the relaxation delay prior to each scan from about 1.2 s to 400 ms. During this time and the FID acquisition (100 ms), only about 50% of the magnetization had relaxed back to $+Z$. Therefore, the optimal first excitation pulse is 120° (see Materials and Methods). The pulse sequence recovers the remaining unexcited magnetization to increase the amount of $+Z$ magnetization for the next scan. The water is flipped back to $+Z$ after every proton pulse to decrease the signal loss of amide protons with high water exchange rates in the intermediate and the native state. The experimental time for one 2D-HMQC experiment under our experimental conditions could thus be reduced to 207 s.

From this 2D real-time NMR experiment, it was possible to fully reconstruct the 2D HMQC spectrum of the folding intermediate (Figure 2B). It was generated by adding the first four 2D spectra recorded during the refolding reaction and by subtracting 21% of the native spectrum (Figure 2A) to account for the fast reaction of U^{39c}. The spectrum exhibits the same dispersion of the resonances and the same line widths as the spectrum of the native state, even though for many residues the exact chemical shift positions of the cross-peaks differ.

Three different time dependencies of cross-peak intensities in the complete 2D HMQC spectra series were observed. Backbone amides of the intermediate with chemical shifts different from the native shifts show a decrease in intensity (Figure 3I). A total of 25 signals without spectral overlap could be analyzed, even though for most signals the assignment is not yet known. Only in a few cases could a decaying signal in close proximity to the native cross-peak [$<$0.05 ppm (^{1}H) and 0.5 ppm (^{15}N)] be assigned to an intermediate backbone residue after inspection of its NOE pattern in the 2D real-time NOESY experiment (*11*). These residues include S13, S37, and G88. On average, single-exponential decay curves with time constants of 390 ± 40 min were observed.

The second class of cross-peaks arises from amides in the native state, which differ in chemical shift from the respective amide in the intermediate state. In the absence of overlap with other signals, the peak intensities of all these amides increased monoexponentially. A total of 44 cross-peaks fulfill this requirement with time constants of 352 ± 31 min. An averaged offset of 21 ± 5% was observed due to U^{39c}, in good agreement with earlier studies (*11, 14*). Time courses with offsets bigger than 30% were excluded from this set. They result most probably from overlap with other signals.

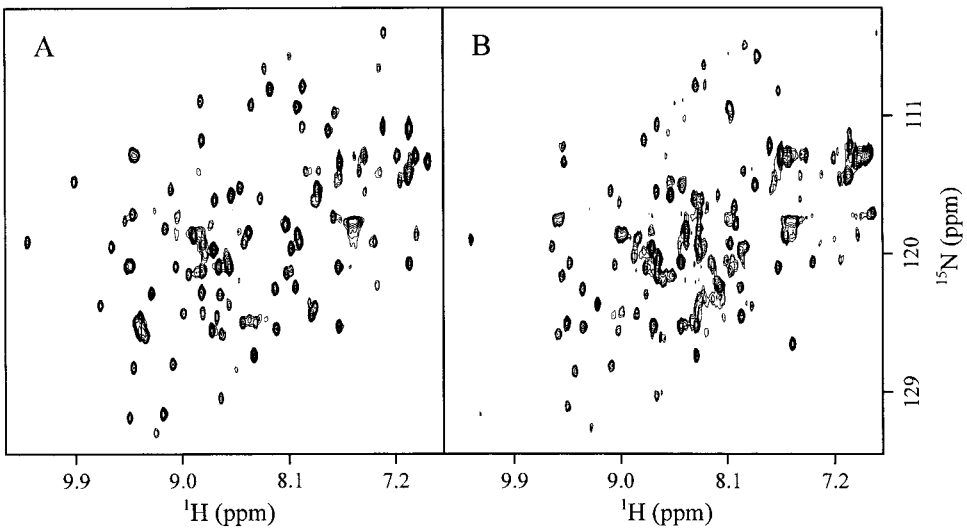

FIGURE 2: Fast ^{15}N-HMQC spectra recorded during refolding of S54G/P55N-RNase T1 from 6 M GdnHCl by 10-fold dilution of (A) the final native state and (B) the folding intermediate. The latter spectrum is a sum of the first four 2D spectra subtracted by 21% of the native spectrum to account for the fast reaction of U^{39c} molecules. Both spectra depict similarly well-dispersed resonances, indicating that the intermediate state contains substantial secondary and tertiary structure.

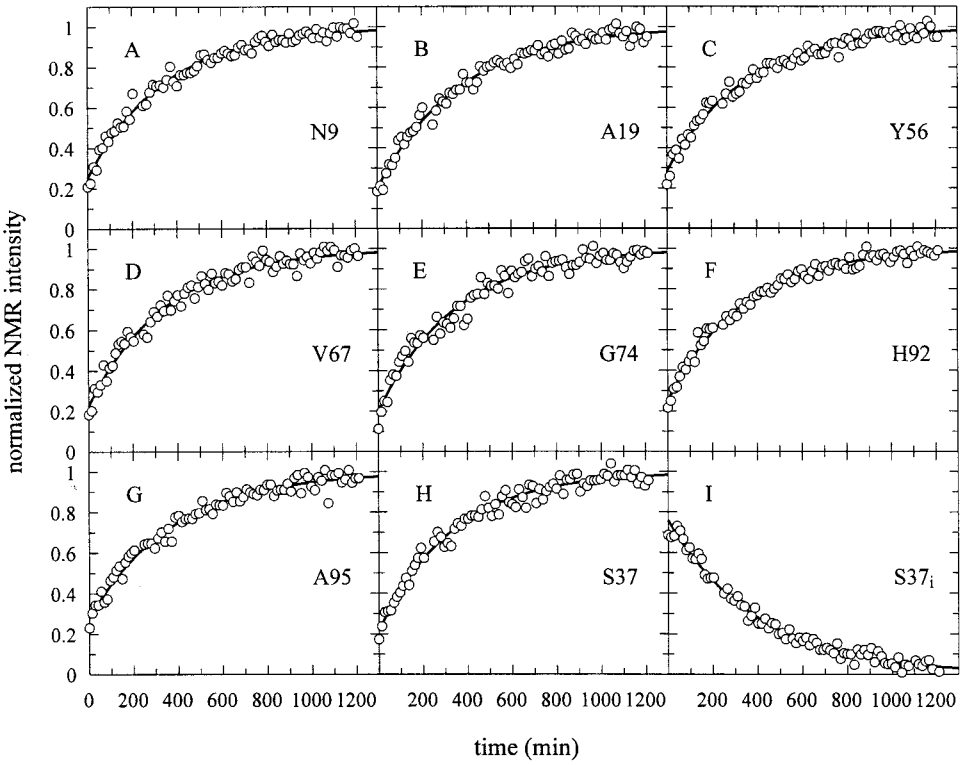

FIGURE 3: Representative refolding kinetics of S54G/P55N-RNase T1 from 6 M GdnHCl monitored by the cross-peak intensities of various residues in a series of 128 fast 2D ^{15}N-HMQC experiments. For the first 16 points, four 2D spectra recorded with 4 scans per t_1 increment were averaged whereas the following 64 experiments were recorded with 16 scans. A single-exponential function was fitted to the intensities with time constants given in Table 1 and (I) 389 ± 15 min for the decaying intensity of the S37 resonance in I^{39t}.

Figure 3 depicts the single-exponential refolding kinetics monitored at eight amides of S54G/P55N-RNase T1. A complete list of time constants for 44 accessible amides is given in Table 1. Within experimental error, all analyzed resonances follow the same single-exponential kinetics, strongly suggesting that the entire protein follows cooperatively the rate-limiting prolyl isomerization.

The third class of cross-peaks comprises 22 resonances, which do not change substantially in their signal intensity during the full experiment. These resonances originate from residues which already have native chemical shifts for both the amide proton and the amide nitrogen nucleus before the slow folding reaction. Therefore, they identify regions in which a native environment is already present in the intermediate state.

These time-resolved 2D NMR experiments provide us with a high-resolution picture of the refolding of S54G/P55N-RNase T1. The intermediate, which is formed in the first, rapid step of folding, is already highly structured and contains several stretches in the native conformation. In the second,

Table 1: Refolding Time Constants Monitored by Individual Amide Protons of S54G/P55N-RNase T1

residue	time constant (min)	residue	time constant (min)	residue	time constant (min)
T5	370 ± 19	L26	328 ± 22	I61	341 ± 41
G7	396 ± 30	H27	320 ± 29	S63	314 ± 21
S8	375 ± 13	D29	408 ± 24	V67	347 ± 18
N9	347 ± 15	G30	391 ± 35	Y68	354 ± 29
S13	280 ± 15	T32	376 ± 15	S69	293 ± 22
D15	375 ± 20	V33	317 ± 21	G71	349 ± 25
V16	377 ± 28	G34	397 ± 25	G74	352 ± 21
S17	358 ± 18	S37	335 ± 16	D76	367 ± 22
T18	334 ± 13	Y38	347 ± 31	R77	358 ± 29
A19	374 ± 17	H40	310 ± 30	V89	410 ± 26
Q20	358 ± 25	N55	358 ± 31	H92	339 ± 13
A21	316 ± 17	Y56	358 ± 17	T93	363 ± 24
A22	379 ± 20	Y57	385 ± 20	A95	379 ± 21
G23	355 ± 33	W59	283 ± 30	C103	345 ± 39
K25	325 ± 36				

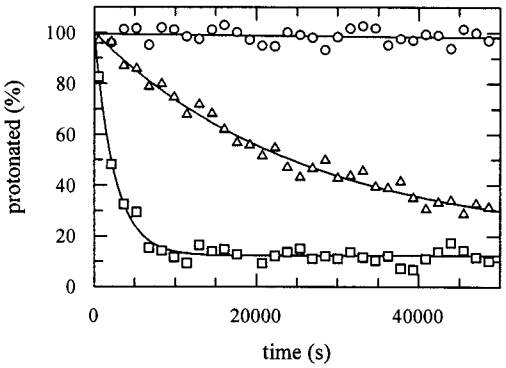

FIGURE 4: Representative decay curves of the proton occupancy for (○) slow (L26), (△) middle (T93), and (□) fast (V52) H/D exchanging protons of protonated S54G/P55N-RNase T1 dissolved in D_2O at 25 °C, pH* 5.0. A single-exponential function was fitted to the data, resulting in 6.0×10^{-6} min^{-1}, 2.3×10^{-3} min^{-1}, and 2.4×10^{-2} min^{-1} exchange rates, respectively. An offset of about 10% was observed due to remaining H_2O in the sample.

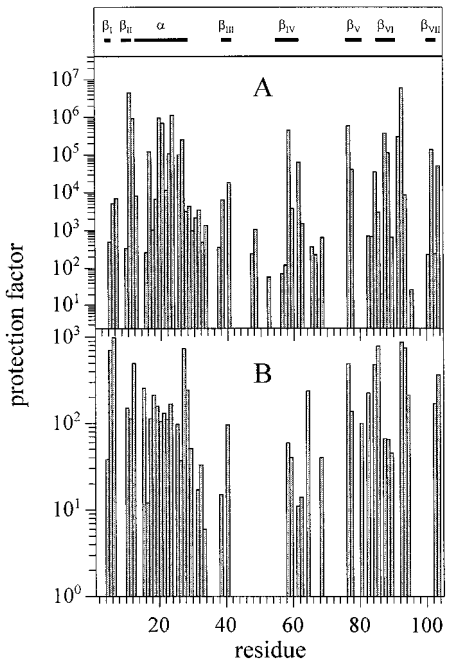

FIGURE 5: Protection factors of (A) native S54G/P55N-RNase T1 at 25 °C, pH 5.0, and (B) the folding intermediate as a function of the residue number. The latter were derived from a competition between H/D exchange and refolding from protonated unfolded protein in 6 M GdnHCl in deuterated refolding buffer, pH 5.0, at 10 °C. Missing bars indicate residues where no data were available. On top, the locations of secondary structure elements along the peptide chain are indicated.

slow step, all the not-yet-native regions follow cooperatively the rate-limiting trans → cis isomerization of peptide bond Tyr38−Pro39.

Protection Factors in the Native State. Hydrogen−deuterium exchange kinetics of amide backbone protons monitored at high resolution by NMR spectroscopy provide valuable information about the local structure and stability. The exchange rates decrease by several orders of magnitude for buried or hydrogen-bonded amide protons when compared to exposed or non-hydrogen-bonded exchangeable protons. Furthermore, they can reflect local or global unfolding events, if the H/D exchange follows the EX2 mechanism. This requires a much faster conformational closing rate in comparison to the exchange rate from the open state and is fulfilled by most proteins studied at low pH.

A total of 128 HMQC spectra were recorded after native protonated protein was dissolved in D_2O, pH* 5.0, to determine the H/D exchange rates of individual backbone amide protons. Figure 4 pictures three representative decay curves for amide protons with high, middle, and low protection. The assigned signals were integrated in the consecutive HMQC spectra, and a single-exponential equation was fitted to the kinetics. Protection factors $P = k_{int}/k_{ex}$ for S54G/P55N-RNase T1 (Figure 5A) were derived by dividing the intrinsic exchange rates (k_{int}) determined from peptide models (*25*) by the experimental exchange rates k_{ex}. In the folded protein, k_{ex} could be determined for the amide protons of 60 residues. They range from 21 for Leu86 to 5.9×10^6 for His92. No value could be determined for residues showing extremely fast exchange rates or missing assignments. Additionally, the protection factor for the side chain $H^{\epsilon 1}$ of Trp59 was determined to be 1.2×10^6. To prove that the H/D exchange follows an EX2 mechanism, a similar experiment was performed at pH 4 (data not shown). The exchange rates decreased as expected by 1 order of magnitude.

The minimal protection factor for residues which require a global unfolding of the entire protein to release the amide proton can be calculated from the Gibbs free energy of unfolding with GdnHCl (eq 2 under Materials and Methods). At 0.6 M GdnHCl, ΔG_D is 32 kJ/mol at 25 °C and pH 5 (*28*), and the respective protection factor is 4×10^5. Only few residues are protected above this value. Nevertheless, they are spread out over the whole protein and are located in secondary structures β II, α, β IV, β V, and β VI. Similar locations were found for wild-type RNase T1 (*29*). One main difference from the wild-type protein is that in the variant the maximal protection factors are more evenly distributed among these structural elements. For the wild-type protein, the α-helix was found to be significantly less protected. This observation was discussed as an increased flexibility of the α-helix compared to the central β-sheet. The second main difference from the wild-type form is that the absolute values of the most protected amide protons in S54G/P55N-RNase T1 are about 2 orders of magnitude smaller. This drop results first from the slightly reduced stability of S54G/P55N-RNase

T1 with respect to its wild-type by about 4 kJ/mol. Second, the presence of 0.6 M GdnDCl (to meet the final conditions of the competition experiment described below) reduces the Gibbs free energy by another 7 kJ/mol.

The unfolding mechanism of S54G/P55N-RNase T1 in strong denaturants has been studied in great detail by Mayr et al. (*16*). They found a slow isomerization of prolyl peptide bond 39 from the less favored cis form to the more favored trans form. Therefore, an additional difference in the free energy has to be taken into account, given by eq 3 (*30*):

$$\Delta\Delta G = \Delta G^0_{op} - \Delta G^0_u = RT \ln(1 + K) \qquad (3)$$

with G^0_{op} the free energy of opening, G^0_u the global free energy, and K the equilibrium constant of the cis/trans isomerization in the unfolded state. At 25 °C, K is 5.3, resulting in an increase in the free energy of 4.6 kJ/mol, equivalent to a maximal protection factor of 2.6×10^6. This is very close to the values we found for the most protected amides of C10 and H92. Therefore, we can exclude an overestimation of the intrinsic exchange rates due to residual structure in the unfolded state. Similar results were found for the wild-type protein, where an exclusion of the latter contribution could be shown experimentally by a temperature-dependent study (*29*).

Competition between Refolding and H/D Exchange. It is difficult to measure protection factors for protein folding intermediates because they are transient species. When, however, H/D exchange and refolding follow similar rates, a competition between both processes can be used to determine the protection factors in intermediate states (*7, 8, 31, 32*). Under the chosen conditions (pH 4.0 and pH 5.0, 10 °C), the rate constant of folding is about 0.01 min^{-1}, and the intrinsic amide proton exchange rates range between 0.1 and 20 min^{-1}. Therefore, the competition experiment is sensitive to moderate protection in the intermediate. In a simplified model, where exchange from the native state can be neglected and where no back-in change of remaining H_2O in the D_2O solution needs to be considered, the protection factor P of an amide proton in the intermediate is given by

$$P = \frac{k_{int} S_{rel}}{k_f (1 - S_{rel})} \qquad (4)$$

In eq 4, k_{int} is the intrinsic exchange rate of the respective peptide (*25*), S_{rel} is the ratio between the cross-peak intensity in the competition experiment and in the reference experiment, and k_f is the refolding rate.

Refolding has been initiated by a 10-fold dilution of protonated unfolded protein in 6 M GdnHCl in deuterated buffer at 10 °C. After the competition experiment was complete, a 2D ^{15}N-HMQC spectrum was recorded. The intensities of the cross-peaks in this spectrum were divided by the intensities of the respective signals in a reference HMQC, where protonated native protein was dissolved in a deuterated buffer under the same conditions as the competition experiment. Figure 5B depicts the protection factors of the intermediate state of S54G/P55N-RNase T1 calculated by using eq 4. The factors range from 6 (V33) to 980 (C6) and are therefore with few exceptions 2 orders of magnitude smaller than the protection factors of the native state, which was the requirement for the calculation of P with eq 4. A comparison with the protected sites in the native state (Figure 5A) shows about the same distribution upon the secondary structure elements of S54G/P55N-RNase T1.

DISCUSSION

The Folding Intermediate Has Almost Native Compactness and Chemical Shift Dispersion. Compaction of the protein chain must occur at some stage during the refolding process starting from the extended unfolded state in high concentration of denaturants. The reduction in the radius of gyration (R_g) upon folding derived from small-angle X-ray scattering (SAXS) depends on the molecular mass for globular proteins and ranges between 60% for a 14 kDa protein and 300% for a 45 kDa protein (*33, 34*). Time-resolved stopped-flow SAXS and stopped-flow dynamic light scattering experiments revealed that compaction can occur early or late during refolding (*33, 35*−*39*) and does not necessarily have to precede the rate-limiting step of folding (*40*).

To determine the hydrodynamic radius of the folding intermediate of S54G/P55N-RNase T1, we used a new real-time NMR diffusion technique. We find that the collapse to an almost native hydrodynamic radius has occurred before the rate-limiting last folding step, the trans → cis isomerization of peptide bond Y38−P39.

The 2D ^{1}H−^{15}N-HMQC spectrum, which could be reconstructed from the real-time NMR experiment (Figure 2B), revealed a very detailed picture of the intermediate. The cross-peaks of all detectable 100 backbone amides are very well dispersed and resemble therefore the spectrum of a protein with strong secondary and tertiary interactions. Only local secondary structure, as in intermediates of the molten globule type, is not sufficient to induce such a good chemical shift dispersion and narrow lines. The 2D ^{1}H−^{15}N-HSQC spectra of the molten globule state of bovine or human α-lactalbumin are poorly resolved, the majority of resonances being broad and clustered between 7.8−8.5 ppm (^{1}H) and 117−122 ppm (^{15}N) (*10, 41*).

The close similarity between the folding intermediate of S54G/P55N-RNase T1 and the native conformation in terms of translational diffusion and its 2D ^{1}H−^{15}N-HMQC spectrum complements earlier observations by circular dichroism spectroscopy (*15*), by 1D real-time NMR spectroscopy, and from the detection of native NOE effects in this state (*11*). Together with a low but significant enzymatic activity (*15*), we can conclude that the compact intermediate has a substantial amount of native secondary and tertiary structure present.

Native Stretches in the Intermediate and Cooperativity during the Rate-Limiting Folding Step. By using conditions where ^{15}N-S54G/P55N-RNase T1 refolds very slowly and a fast acquisition of a series of 2D NMR spectra, the time course of folding could be monitored for the majority of backbone amides; 66 belong to cross-peaks of the native state with known assignment. For most of the resolved 25 signals of the intermediate state, the assignment is not yet known. Two sets of native cross-peaks could be defined according to their time course in the set of spectra. The intensity of 22 cross-peaks did not change during the whole experiment, which indicates that they have identical chemical shifts in the intermediate and native state. These residues thus identify a nativelike environment in the intermediate, which defines

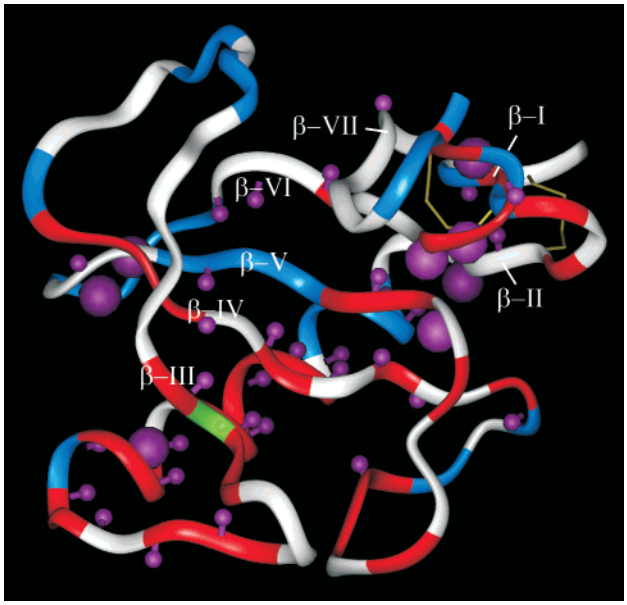

FIGURE 6: Backbone diagram of S54G/P55N-RNase T1 based on X-ray data (Hinrichs et al., unpublished results). Red sections indicate residues with not-yet-native chemical shifts of the backbone amides in the folding intermediate of S54G/P55N-RNase T1, whereas blue sections highlight residues with native chemical shifts in the intermediate. The two disulfide bonds (Cys2−Cys10 and Cys6−Cys103) are colored yellow; Pro39 is given in green; and for white stretches, no unambiguous data were available. Large spheres represent backbone amide protons with strong protection factors in the intermediate ($P > 300$), small spheres amide protons with weak and medium protection ($10 \leq P \leq 300$). This figure was produced by using INSIGHT II (MSI).

very sensitively the chemical shifts of the amide proton and the corresponding ^{15}N nucleus.

In Figure 6, these native stretches in the intermediate are colored in blue. They comprise most of β-strand I, the N-terminal part of the α-helix, the turn between β-strands III and IV (for this region, no data were accessible from the 2D real-time NOESY experiment), the N-terminal part of the loop between β-strands IV and V, β-strand V, and the loops between β-strands V and VI and β-strands VI and VII. These native regions in the intermediate correspond and complement the native regions in I^{39t} determined earlier by a 2D real-time NOESY experiment (*11*). It should be noted that these native regions are not all located in regular secondary structure elements of the final native state. They can form at independent positions including later loops and turns.

The second set of 44 native cross-peak showed an increase in intensity with time in the series of 2D spectra. They indicate regions where a not-yet-native environment in the intermediate results in different chemical shifts with respect to the native state. In Figure 6, they are colored red and include the turn between β-strands I and II, the C-terminal part of the α-helix and the following loop, β-strand III, β-strand IV (for this region, no data were accessible from the 2D real-time NOESY experiment), and the C-terminal part of the loop between β-strand IV and β-strand V.

The analysis of these 44 time courses revealed that all time constants fall into the same range of 352 ± 31 min with an amplitude offset of 21 ± 5%. Together with the averaged time constants of the 25 accessible decaying intermediate signals of 390 ± 9 min, we can conclude that the rate-limiting refolding step from the intermediate to the native state is a highly cooperative reaction. The slow trans → cis isomerization of prolyl peptide bond 39 of S54G/P55N-RNase T1 thus synchronizes the refolding reaction for all regions, which are not yet in a native conformation in the intermediate state. These stretches not only are in close proximity to peptide bond Y38−P39 but also cover the entire protein chain. This agrees with the conclusion drawn from the kinetic analysis of a few resolved proton resonances in the same refolding experiment at 10 °C monitored by a series of 1D spectra (*11*).

Refolding from the kinetic and the equilibrium molten globule of bovine α-lactalbumin to the native state revealed a high cooperativity as well (*10*, *42*), whereas, for example, the refolding of the four domain protein annexin 1 (*43*), refolding of hen egg white or equine lysozyme (*4*, *31*, *44*), refolding of ribonuclease A (*6*), and unfolding of the molten globule of human α-lactalbumin (*41*) are mainly noncooperative folding reactions.

The high number of not-yet-native chemical shifts in the intermediate of S54G/P55N-RNase T1 with the non-native trans prolyl peptide bond is very distinct from the results for C40/82A P27A barstar (*45*). Killick et al. followed the refolding of this protein by a set of 16 2D ^{1}H−^{15}N-HSQC spectra in a real-time NMR study, and found only local changes around the non-native Pro 48 in an intermediate with a predominantly native NMR spectrum.

Hydrogen Exchange in Native S54G/P55N-RNase T1. In the native state of S54G/P55N-RNase T1, 41 of the assigned amide protons are involved in hydrogen bonds also found in the wild-type protein (*46*). From these 41 protons, 40 show protection from exchange in the variant (Figure 5A). The only exception is F50, which was not significantly protected in the wild-type protein as well (*29*). Another 20 residues not involved in hydrogen bonding show reduced exchange rates. In general, the protection pattern of S54G/P55N-RNase T1 matches closely the pattern observed for the wild-type protein (*29*).

In all regular secondary structure elements, amides with protection factors above 10^4 were found. C10 involved in a disulfide bond and H92 at the C-terminal end of β-strand V show maximal values above 5×10^6. The hydrogen bonding network of β-strand III following mutation site 54−55 is also not affected.

Groups of residues with significantly reduced protection factors in the hydrogen bonding network were found in β-strand I close to the N-terminus, at the C-terminus of the α-helix and in the following loop, in β-strand III, and in two loop regions between β III/IV and β IV/V. All these sections are exposed to the surface of the protein. Here, the exchange with the solvent does not require a global unfolding of the entire protein chain. A direct comparison with the protection in the wild-type protein in these regions is only possible for β-strand I, where similarly decreased factors were found. For the remaining regions, no protection factors could be derived by Mullins et al. mainly because of a lower resolution in their homonuclear NMR study (*29*).

Pfeiffer et al. determined those amide protons in wild-type RNase T1 which show fast exchange with water (*47*). None of these 24 fast exchanging protons showed detectable protection in the variant. Seven out of eight amide protons,

which were found in the same study to interact with water molecules with increased residence times, are protected in the variant.

Together with the close resemblance between the X-ray structures of wild-type RNase T1 (*48*) and S54G/P55N-RNase T1 (Hinrichs et al., unpublished results), we can conclude that the characteristic of the variant structure is very close to the wild-type structure and that mutations S54G and P55N of a cis prolyl peptide bond in the wild-type to a trans peptide bond in the variant have only local effects.

High Protection Factors in the Folding Intermediate. Protection factors of the folding intermediate of S54G/P55N-RNase T1 could be determined by a competition between the H/D exchange and the refolding reaction. In two regions of the intermediate, strong protection with factors higher than 300 was found. They are illustrated in the native structure in Figure 6 by large spheres and comprise the amide protons of residues H27, N84, and Q85 at one side of the central β-sheet and T5, C6, S12, D76, H92, T93, and C103 at the other side close to the disulfide bonds connecting the termini. An average protection value of 660 for these 10 residues corresponds to a stabilization free energy of 15 kJ/mol (10 °C, 0.6 M GdnDCl) for the intermediate. Under these conditions, the folded state is stabilized by 40 kJ/mol (*15*), indicating that the intermediate has already reached about 40% of the final free energy gain. This is a remarkably high value compared to folding intermediates of other proteins. For example, apoplastocyanin of French bean, which also forms an intermediate with an incorrect trans prolyl peptide bond, shows only weak protection with factors on the order of 5−50 (*32*). In horse cytochrome *c*, protection factors range between 0.5 and 4.8 for the burst intermediate (*49*), between 20 and 200 for early states in T4 lysozyme refolding (*50*), and between 10 and 60 for intermediates of staphylococcal nuclease (*50, 51*). The burst phase intermediate of ribonuclease A revealed protection factors in the rage of 10−100, which exceed 1000 at 400 ms refolding time (*6*). A more detailed mathematical description of amide protection in very early kinetic folding intermediates has been given recently (*52*).

That the folding polypeptide chain of S54G/P55N-RNase T1 with the non-native trans prolyl peptide bond 39 needs to gain another 25 kJ/mol to reach the native conformation is also distinct from proteins such as staphylococcal nuclease (*53*), calbindin (*54*), and several others that exist as mixtures of nativelike conformations with alternative prolyl isomers but with very similar energy.

Amide protons with protection factors between 10 and 300 are indicated in Figure 6 by small spheres. They are evenly distributed over the whole structure. No protected residues were found in the long loop between β-strands III and IV, where even the native state shows only weak protection. Four regions are less reduced in their stability in the intermediate compared to the overall reduction: β-strand I, the C- and N-terminii of the α-helix, and residues 82, 84, and 85.

Mullins et al. determined in wild-type RNase T1 24 rapidly protected backbone amides during 8 ms to 10 s of refolding in an H/D pulse labeling experiment (*55*). Nineteen could be analyzed here in the intermediate of S54G/P55N-RNase T1 as well. They exhibit various protection factors without preferences to one of the two intermediates proposed by the authors according to early and late protection within their time window.

Several backbone amides, e.g., in the central part of the α-helix or β-strand IV, show strong protection in both the intermediate and the native state, but lack native chemical shifts in the intermediate state. This is a surprising result. We suggest that these regions form not-yet-native secondary and tertiary structures which protect the amide protons, but which need to rearrange in the subsequent folding reaction. On the contrary, unprotected stretches such as the loop between β-strands III and IV can form a native conformation as judged from the chemical shifts in I^{39t}. These findings show that models for the succession of folding events purely derived from amide protection data in intermediates can be incomplete.

Conclusions. The application of high-resolution 2D NMR techniques enabled us to characterize the stability of a folding intermediate and its reaction to the native state at an unprecedented molecular resolution. In particular, the kinetics of folding of our model protein S54G/P55N-RNase T1 could be studied based on 66 local reporter groups covering all sites of the polypeptide chain. Together with the real-time diffusion experimnets and the amide protection factors of the intermediate, we are able to sketch the following folding scenario of S54G/P55N-RNase T1.

In the first, rapid step of folding (which occurs in the dead-time of the real-time NMR experiments), the molecules with non-native trans prolyl peptide bond 39 form a compact intermediate stabilized by 15 kJ/mol. The slow folding reaction from the intermediate to the native state is a fully synchronized, cooperative process. The rate-limiting trans → cis isomerization at Pro39 controls the rate of folding at all 66 NH positions. In the intermediate state, native and not-yet-native regions are formed at various sites, all containing substantial secondary and tertiary structure interactions and tolerating trans Y38−P39. The native regions are not confined to well-defined secondary structure elements of the later native state but include also connecting loops.

Highly structured intermediates with non-native prolyl peptide bonds probably occur in vivo as well. After synthesis at the ribosome, the peptide chain can fold rapidly to a globular intermediate, which buries hydrophobic regions and thus prevents aggregation. The final proline-limited step of folding can then be catalyzed by one of the ubiquitous peptidyl-prolyl-isomerases.

ACKNOWLEDGMENT

We thank W. D. Schubert, U. Hahn, and W. Saenger for providing us with the clone of the S54G/P55N mutant of RNase T1 and for the X-ray coordinates, P. Rösch for NMR time at the DRX 600, A. Ross (Hoffmann-LaRoche, Basel) for discussions about fast HMQC experiments, and F. X. Schmid for very helpful general discussions.

REFERENCES

1. Eaton, W. A., Munoz, V., Thompson, P. A., Chan, C.-K., and Hofrichter, J. (1997) *Curr. Opin. Struct. Biol. 7*, 10−14.
2. Udgaonkar, J. B., and Baldwin, R. L. (1988) *Nature 335*, 694−699.
3. Roder, H., Elöve, G. A., and Englander, S. W. (1988) *Nature 335*, 700−704.

4. Radford, S. E., Dobson, C. M., and Evans, P. A. (1992) *Nature 358*, 302−307.
5. Jennings, P. A., and Wright, P. E. (1993) *Science 262*, 892−896.
6. Udgaonkar, J. B., and Baldwin, R. L. (1990) *Proc. Natl. Acad. Sci. U.S.A. 87*, 8197−8201.
7. Roder, H., and Wüthrich, K. (1986) *Proteins: Struct., Funct., Genet. 1*, 34−42.
8. Schmid, F. X., and Baldwin, R. L. (1979) *J. Mol. Biol. 133*, 285−287.
9. van Nuland, N. A. J., Forge, V., Balbach, J., and Dobson, C. M. (1998) *Acc. Chem. Res. 31*, 773−780.
10. Balbach, J., Forge, V., Lau, W. S., van Nuland, N. A. J., Brew, K., and Dobson, C. M. (1996) *Science 274*, 1161−1163.
11. Balbach, J., Steegborn, C., Schindler, T., and Schmid, F. X. (1999) *J. Mol. Biol. 285*, 829−842.
12. Hoeltzli, S. D., and Frieden, C. (1996) *Biochemistry 35*, 16843−16851.
13. Ross, A., Salzman, M., and Senn, H. (1997) *J. Biomol. NMR 10*, 389−396.
14. Kiefhaber, T., Grunert, H.-P., Hahn, U., and Schmid, F. X. (1990) *Biochemistry 29*, 6475−6480.
15. Kiefhaber, T., Schmid, F. X., Willaert, K., Engelborghs, Y., and Chaffotte, A. (1992) *Protein Sci. 1*, 1162−1172.
16. Mayr, L. M., Odefey, C., Schutkowski, M., and Schmid, F. X. (1996) *Biochemistry 35*, 5550−5561.
17. Quaas, R., McKeown, Y., Stanssens, P., Frank, R., Blöcker, H., and Hahn, U. (1988) *Eur. J. Biochem. 173*, 617−622.
18. Mayr, L. M., and Schmid, F. X. (1993) *J. Mol. Biol. 231*, 913−926.
19. Marion, D., Ikura, M., Tschudin, R., and Bax, A. (1989) *J. Magn. Reson. 85*, 393−399.
20. Kay, L., Keifer, P., and Saarinen, T. (1992) *J. Am. Chem. Soc. 114*, 10663−10665.
21. Gibbs, S. J., and Johnson, C. S., Jr. (1991) *J. Magn. Reson. 93*, 395−402.
22. Jones, J. A., Wilkins, D. K., Smith, L. J., and Dobson, C. M. (1997) *J. Biomol. NMR 10*, 199−203.
23. Palmer, A. G., III, Cavanagh, J., Wright, P. E., and Rance, M. (1991) *J. Magn. Reson. 93*, 151−170.
24. Schleucher, J., Schwendinger, M., Sattler, M., Schmidt, P., Schedletzky, O., Glaser, S. J., Sørensen, O. W., and Griesinger, C. (1994) *J. Biomol. NMR 4*, 301−306.
25. Bai, Y. W., Milne, J. S., Mayne, L., and Englander, S. W. (1993) *Proteins: Struct., Funct., Genet. 17*, 75−86.
26. Pfeiffer, S., Engelke, J., and Rüterjans, H. (1996) *Q. Magn. Res. Biol. Med. 3*, 69−87.
27. Stejskal, E. O., and Tanner, J. E. (1965) *J. Chem. Phys. 42*, 288−292.
28. Kiefhaber, T., and Schmid, F. X. (1992) *J. Mol. Biol. 224*, 231−240.
29. Mullins, L. S., Pace, C. N., and Raushel, F. M. (1997) *Protein Sci. 6*, 1387−1395.
30. Bai, Y. W., Milne, J. S., Mayne, L., and Englander, S. W. (1994) *Proteins: Struct., Funct., Genet. 20*, 4−14.
31. Miranker, A., Radford, S. E., Karplus, M., and Dobson, C. M. (1991) *Nature 349*, 633−636.
32. Koide, S., Dyson, H. J., and Wright, P. E. (1993) *Biochemistry 32*, 12299−12310.
33. Arai, M., Ikura, T., Semisotnov, G. V., Kihara, H., Amemiya, Y., and Kuwajima, K. (1998) *J. Mol. Biol. 275*, 149−162.
34. Kataoka, M., Kuwajima, K., Tokunaga, F., and Goto, Y. (1997) *Protein Sci. 6*, 422−430.
35. Eliezer, D., Jennings, P. A., Wright, P. E., Doniach, S., Hodgson, K. O., and Tsuruta, H. (1995) *Science 270*, 487−488.
36. Semisotnov, G. V., Kihara, H., Kotova, N. V., Kimura, K., Amemiya, Y., Wakabayashi, K., Serdyuk, I. N., Timchenko, A. A., Chiba, K., Nikaido, K., Ikura, T., and Kuwajima, K. (1996) *J. Mol. Biol. 262*, 559−574.
37. Gast, K., Nöppert, A., Müller-Frohne, M., Zirwer, D., and Damaschun, G. (1997) *Eur. Biophys. J. 25*, 211−219.
38. Nöppert, A., Gast, K., Zirwer, D., and Damaschun, G. (1998) *Folding Des. 3*, 213−221.
39. Segel, D. J., Bachmann, A., Hofrichter, J., Hodgson, K. O., Doniach, S., and Kiefhaber, T. (1999) *J. Mol. Biol. 288*, 489−499.
40. Plaxco, K. W., Millett, I. S., Segel, D. J., Doniach, S., and Baker, D. (1999) *Nat. Struct. Biol. 6*, 554−556.
41. Schulman, B. A., Kim, P. S., Dobson, C. M., and Redfield, C. (1997) *Nat. Struct. Biol. 4*, 630−634.
42. Balbach, J., Forge, V., van Nuland, N. A. J., Winder, S. L., Hore, P. J., and Dobson, C. M. (1995) *Nat. Struct. Biol. 2*, 865−870.
43. Cordier-Ochsenbein, F., Guerois, R., Russo-Marie, F., Neumann, J. M., and Sanson, A. (1998) *J. Mol. Biol. 279*, 1177−1185.
44. Morozova-Roche, L. A., Jones, J. A., Noppe, W., and Dobson, C. M. (1999) *J. Mol. Biol. 289*, 1055−1073.
45. Killick, T. R., Freund, S. M., and Fersht, A. R. (1999) *Protein Sci. 8*, 1286−1291.
46. Pace, C. N., Heinemann, U., Hahn, U., and Saenger, W. (1991) *Angew. Chem., Int. Ed. Engl. 30*, 343−360.
47. Pfeiffer, S., Spitzner, N., Löhr, F., and Rüterjans, H. (1998) *J. Biomol. NMR 11*, 1−15.
48. Heinemann, U., and Saenger, W. (1982) *Nature 299*, 27−31.
49. Sauder, J. M., and Roder, H. (1998) *Folding Des. 3*, 293−301.
50. Lu, J. R., and Dahlquist, F. W. (1992) *Biochemistry 31*, 4749−4756.
51. Guijarro, J. I., Jackson, M., Chaffotte, A. F., Delepierre, M., Mantsch, H. H., and Goldberg, M. E. (1995) *Biochemistry 34*, 2998−3008.
52. Houry, W. A., Sauder, J. M., Roder, H., and Scheraga, H. A. (1998) *Proc. Natl. Acad. Sci. U.S.A. 95*, 4299−4302.
53. Chazin, W. J., Kördel, J., Drakenberg, T., Thulin, E., Brodin, P., Grundström, T., and Forsén, S. (1989) *Proc. Natl. Acad. Sci. U.S.A. 86*, 2195−2198.
54. Evans, P. A., Dobson, C. M., Kautz, R. A., Hatfull, G., and Fox, R. O. (1987) *Nature 329*, 266−268.
55. Mullins, L. S., Pace, C. N., and Raushel, F. M. (1993) *Biochemistry 32*, 6152−6156.

BI000270U